

# The Multiband Emission of the two-component Gamma-Ray Burst jet influenced by progenitor winds within the Accretion Disk of Active Galactic Nuclei

HAO-YU YUAN<sup>1</sup> AND WEI-HUA LEI <sup>1</sup>

<sup>1</sup>*Department of Astronomy, School of Physics, Huazhong University of Science and Technology, Luoyu Road 1037, Wuhan, 430074, China*

## ABSTRACT

Gamma-ray bursts (GRBs), both from merger of binary compact objects (short GRBs) and collapse of massive stars (long GRBs), are expected to occur in the dense environments, e.g., the accretion disk of active galactic nuclei (AGN). The propagating of GRB jets in such dense environment will result in multiband transients. Investigating the properties of these transients plays important roles in their identification, understanding the jet structure and constraining population of the star and compact object in AGN disks. In this work, we intend to study the propagation and emission of a two-component GRB jet (a fast narrow component and wide slow one) in the AGN disk. We consider the influence of wind from the short and long GRB progenitors, which would reconstruct the surrounding density distribution and form a cavity in the AGN disk. We find that the long GRB jets will be choked, the dynamics and the emission are resemble to the case without cavity. The narrow and wide cocoon breakout emission can be detected by EP and HXMT, respectively. For short GRBs, we expect a non-thermal afterglow emission from the wide jet and a cocoon breakout emission from the choked narrow jet, which can be monitored by EP and HXMT, respectively. Therefore, the joint observations by EP and HXMT might be helpful to distinguish the type of GRBs in the AGN disk and the jet components.

*Keywords:* [gamma ray burst \(629\)](#), [Galaxy accretion disks \(562\)](#)

## 1. INTRODUCTION

The activity of galactic nuclei (AGN) is believed to be fueled by the accretion of dense matter of the disk onto the central supermassive black hole (SMBH) (Lynden-Bell 1969; Shakura & Sunyaev 1973; Sirko & Goodman 2003). The recent observations suggest that AGN disks constitute dense environments harboring stars and compact objects. The Laser Interferometer Gravitational Wave Observatory (LIGO) has successfully detected a gravitational wave (GW) signal GW190521 from the merger of binary black holes (BBHs) (Abbott et al. 2020). Typically, BBH mergers do not produce electromagnetic (EM) counterparts unless there is an accompa-

nying presence of gas (McKernan et al. 2019). However, approximately 34 days following the GW190521 trigger, the Zwicky Transient Facility (ZTF) detected a potential optical electromagnetic counterpart, ZTF19abanrhr, which exhibited consistency with a plausible association between the GW event and the AGN J14942.3+344929 (Graham et al. 2020; Ashton et al. 2021; Nitz & Capano 2020)<sup>1</sup>.

Stars can be developed inside AGN disks in two ways: gravitational instability within the disk (Paczynski 1978; Goodman 2003; Dittmann & Miller 2020), or capture from the surrounding star cluster (Artymowicz et al.

<sup>1</sup> Recently, the association between GW190521 and ZTF19abanrhr was reanalyzed by Morton et al. (2023) within the Bayesian framework, utilizing the GWTC-2.1 data release (Abbott et al. 2024).

1993; Fabj et al. 2020). A stellar population capable of producing compact objects, such as neutron stars (NSs) and black holes (BHs), upon their deaths. Gamma-ray burst (GRB) jets can be generated in the accretion disk due to the collapse of massive stars or the merger of binary compact objects (Branch & Wheeler 2017; Woosley 1993, BCOs). The connections of long duration GRBs (LGRBs) with core-collapse of massive stars, and short duration GRBs (SGRBs) with the mergers of BCOs have been supported by observations. Zhu et al. (2021) have analyzed the jet produced by the merging of binary neutron stars in the AGN disk. They pointed out that the jet can not successfully break through the surface of the disk and will develop a hot cocoon, which can produce X-ray radiation brighter than the disk itself when the cocoon breaks through the disk surface. These X-ray transients can last  $\sim 1000$  seconds (Chen & Dai 2024; Tagawa et al. 2024). Perna et al. (2021) argued that the GRB jet is harder to break through the disk around a more massive central SMBH. In addition to cocoon shock breakout, shock emission due to the interaction between jet and disk material will diffuse in the disk and produce supernova-like radiation as it emerges from the dense gas (Chatzopoulos et al. 2012; Li et al. 2023). The detailed inspection of these transients would be beneficial in identifying their physical origin and calibrating the populations of stars and compact objects in the AGN disk environment.

The studies mentioned above exclusively employ a simplistic uniform jet model (Zhu et al. 2021; Perna et al. 2021; Chen & Dai 2024; Tagawa et al. 2024). However, theoretical and observational studies revealed that at least some GRB jets could be structured (Zhang et al. 2004; Mészáros et al. 1998; Dai & Gou 2001). Among which, the two-component jet has been widely mentioned (Berger et al. 2003; Sheth et al. 2003; Huang et al. 2004; Wu et al. 2005; Xie et al. 2012; Xu et al. 2000), e.g., the "brightest of all time" burst GRB 221009A (Zheng et al. 2024), which contain a narrow, highly relativistic component and a wider, moderately relativistic component. Exploring the emergent emission of GRBs with two-component jets within AGN disks holds promise for enhancing our comprehension of nuclear transients.

On the other hand, both GRB progenitors (massive star and BCOs) will produce a wind. This wind interacts with the matter in the disk, exerting pressure and causing it to reach an equilibrium at some distance. Es-

pecially for SGRBs, the super-Eddington accretion of the compact objects in a dense environment might lead to a strong wind, which may penetrate the AGN disk. In such case, GRBs could be detected as if they were occurring in a less dense environment (Chen et al. 2023). Therefore, the wind would reconstruct the surrounding density distribution of disk, and should be seriously considered when modeling. Li et al. (2023) analyzed the effect of the wind cavity, but for supernova (SN) radiation in the AGN disk. The study of the influence of the winds on the dynamics and emission for GRB in AGN disk is highly desired, which enable us to compare the predictions from disk SGRBs and LGRBs.

Inspired by these considerations, in this paper, we intend to study the properties of multiband emission from a GRB with two-component jet in AGN disk environment by considering the effects of progenitor wind. The paper is organized as follows. In Section 2, we describe the cavity induced by the progenitor wind of SGRB and LGRB, respectively. In Section 3, we present the dynamics and radiation of a GRB with a two-component jet launched in the AGN disk cavity. The results are presented in Section 4. Finally, Section 5 summarizes and discusses our results.

## 2. GRB PROGENITOR WIND AND CAVITY INDUCED IN AGN DISK

The environment for GRBs in AGN disk differs significantly from interstellar medium (ISM). The dense gas suppresses the GRB jet, leaving a cocoon in the disk (Zhu et al. 2021). On the other hand, the GRB progenitor wind interacts with the disk material, reconstructing the surrounding density configuration. In this section, we will investigate the surrounding environment for SGRBs and LGRBs in AGN disk, respectively.

### 2.1. The AGN Disk Structure

We adopt the standard AGN disk model described in Sirko & Goodman (2003), which includes the gravitational instability and auxiliary heating from nuclear fusion in the disk stars. The  $\alpha$  prescription for the viscosity is adopted. The total luminosity of AGN disk radiation is related to the accretion rate  $\dot{M}_{\text{SMBH}}$  as  $L_0 = \epsilon_d \dot{M}_{\text{SMBH}} c^2$ , and  $l_E = L_0 / L_{\text{Edd}}$  is the ratio of the accretion luminosity and the Eddington luminosity. the Eddington luminosity  $L_{\text{Edd}} = 4\pi G M_{\text{SMBH}} m_p c / \sigma_T$ , where  $G$  is the gravitational constant,  $M_{\text{SMBH}}$  is the mass of

SMBH,  $m_p$  is the mass of proton and  $\sigma_T$  is thomson cross section. The inner ( $R_{\min}$ ) and outer ( $R_{\max}$ ) boundaries of the accretion disk are set to  $R_{\min} = R_s/(4\epsilon_d)$  and  $R_{\max} = 10^6 R_s$ , respectively, where  $R_s = \frac{2GM_{\text{SMBH}}}{c^2}$  is the Schwarzschild radius. In the following calculation, we use  $\alpha = 0.01$ ,  $\epsilon_d = 0.1$ ,  $M_{\text{SMBH}} = 10^8 M_\odot$  and  $l_E = 0.5$ .

The inner disk is powered entirely by gravitational energy, and the relevant equations of the structure are given by (Sirko & Goodman 2003),

$$\sigma_{\text{SB}} T_{\text{d,eff}}^4 = \frac{3}{8\pi} \dot{M}' \Omega_d^2, \quad (1)$$

$$T_d^4 = \left( \frac{3}{8\tau_d} + \frac{1}{2} + \frac{1}{4\tau_d} \right) T_{\text{d,eff}}^4, \quad (2)$$

$$c_s^2 \Sigma_d = \frac{\dot{M}' \Omega_d}{3\pi\alpha}, \quad (3)$$

$$c_s^2 = \frac{P_{\text{gas}} + P_{\text{rad}}}{\rho_d}, \quad (4)$$

where  $T_{\text{d,eff}}$  is the effective temperature,  $T_d$  is the mid-disk temperature,  $\tau_d = \frac{\kappa_d \Sigma_d}{2}$  is the optical depth from the middle to the surface of AGN disk,  $\kappa_d$  is the opacity of the middle disk,  $\rho_d$  is the mid-plane density,  $\Sigma_d = 2\rho_d H$  is the surface density,  $H = \frac{c_s}{\Omega_d}$  is the scale height of the disk,  $P_{\text{rad}} = \frac{\tau_d \sigma_{\text{SB}}}{2c} T_{\text{d,eff}}^4$  is the mid-disk radiation pressure,  $P_{\text{gas}} = \frac{\rho_d k_B T_d}{m_d}$  is the mid-disk gas pressure,  $\Omega_d = (GM_{\text{SMBH}}/R^3)^{1/2}$  is the angular frequency,  $\dot{M}' = \dot{M}_{\text{SMBH}}(1 - \sqrt{R_{\min}/R})$  and  $m_d = 0.62m_p$  is the mean molecular mass. We assume the viscosity is proportional to total pressure within above equations. To simplify the calculation, we use the average opacity given in the standard disk model,  $\kappa_d = \kappa_{\text{es}} + \kappa_0 \rho_d T_d^{-3.5}$ , where  $\kappa_{\text{es}} = 0.4 \text{ cm}^2 \text{ g}^{-1}$  and  $\kappa_0 = 6.4 \times 10^{22} \text{ cm}^2 \text{ g}^{-1}$ .

For the outer disk, the influence of self-gravity of the AGN disk becomes more important. The stability is described with the Toomre's parameter,

$$Q = \frac{c_s \Omega_d}{\pi G \Sigma_d} \approx \frac{\Omega_d^2}{2\pi G \rho_d}. \quad (5)$$

If  $Q \leq 1$ , the gas will become unstable due to the self-gravity and lead to the star formation in AGN disk. Following Sirko & Goodman (2003), additional heating (such as nuclear fusion inside the star) is considered such that  $Q = Q_{\min} \approx 1$ . Then we can replace Eq.1 with

$$\rho_d = \frac{\Omega_d^2}{2\pi G Q_{\min}}, \quad (6)$$

for outer disk. By solving these equations, we can obtain the structure and properties of the inner and outer disk regions. The results are shown in Fig.1.

As we can see, the disk density is  $R$ -dependent. We need to determine the possible location of the GRBs  $R_{\text{GRB}}$  in the disk. Massive stars would migrate inward after forming in the outer region of the AGN disk (Lin & Papaloizou 1993). Li et al. (2023) demonstrate that the migration distance is relatively small and the collapse of massive stars usually occurs at  $\sim 1000R_s$ , which is taken as the location of LGRBs in the AGN disk.

For the SGRB progenitor, we should take into account the further migration of binary compact objects resulting from the collapse of massive stars. Such migration will terminate at migration traps  $\sim 500R_s$ , which would be the location for SGRBs in AGN disk (Bellovary et al. 2016).

Fig.1 reveals that the AGN disk exhibits comparable magnitudes in terms of its height, density, and sound velocity at these two positions (i.e.,  $1000R_s$  for LGRBs and  $500R_s$  for SGRBs). For simplicity, we adopt  $H \sim 10^{14} \text{ cm}$ ,  $\rho_d \sim 10^{-10} \text{ g cm}^{-3}$  and  $c_s \sim 5 \times 10^6 \text{ cm s}^{-1}$  at the disk location of both short and long GRBs in the following calculations.

## 2.2. The Cavity Induced by GRB Progenitor Wind

As the progenitor of LGRBs, a massive star produce strong stellar wind from its surface (Maeder 1983). For binary NSs or NS-BH binaries (as the progenitor of SGRBs), violent wind can be launched from the accretion disk during the hyper Eddington accretion process (Tetarenko et al. 2018).

Now, we consider the interactions between the GRB progenitor wind and the AGN disk gas, which will change the density distribution of the surrounding disk material. The wind would blow the material into a low-density region, called a cavity (Branch & Wheeler 2017). We will study the cavity produced by the two types of GRB progenitor, respectively.

### 2.2.1. Wind from SGRB progenitor

First, we investigate the wind emanating from the SGRB progenitor, i.e., BCOs. We consider a binary composed of two compact stars of equal mass, that is,  $m_1 = m_2$ , and total mass  $m_b = m_1 + m_2 \approx 5M_\odot$ . They are intially orbiting around the SMBH at approximately  $R_{\text{GRB}} \sim 500R_s$  in the AGN disk. The separation

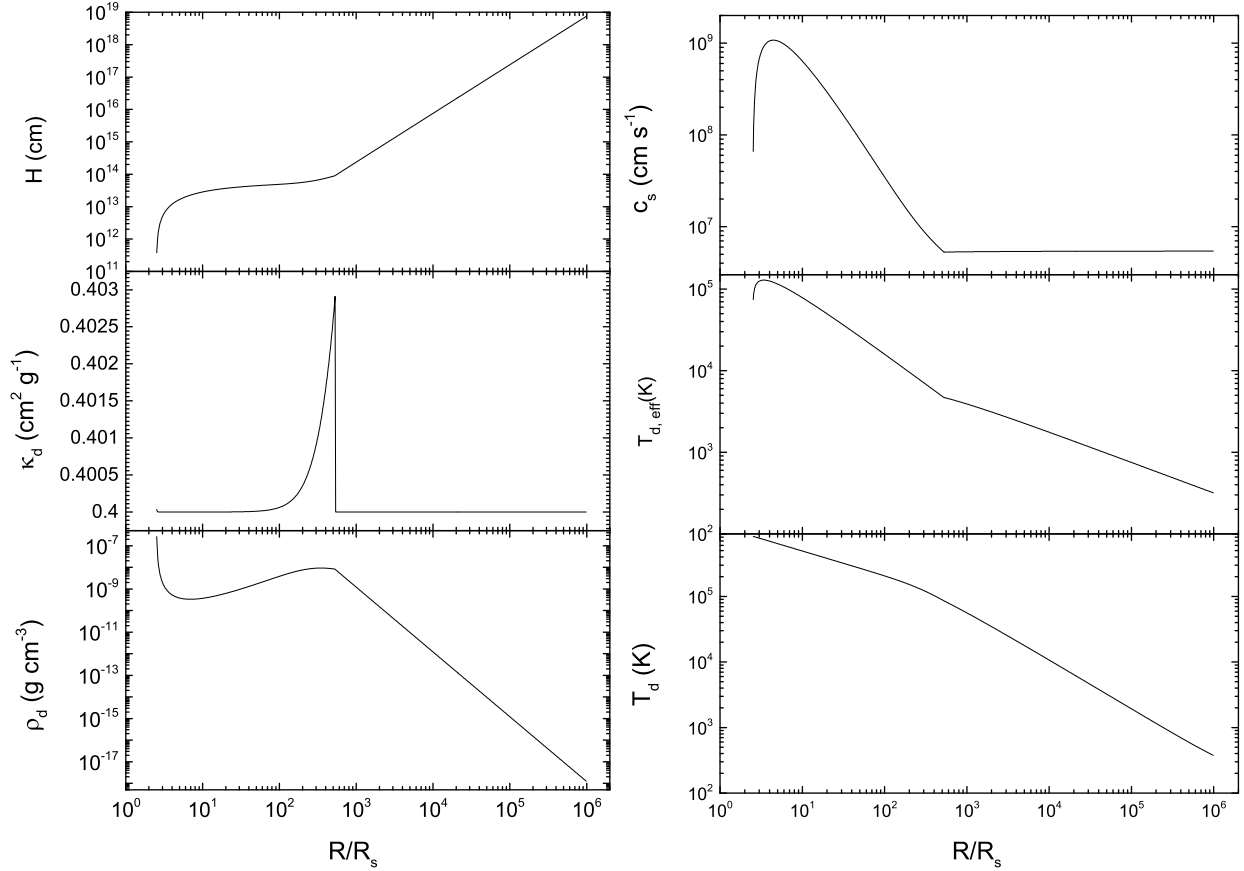


**Figure 1.** The scale height of the AGN disk ( $H$ ), opacity of the middle disk ( $\kappa_d$ ), the mid-plane density ( $\rho_d$ ), the mid-plane sound velocity ( $c_s$ ), the effective temperature ( $T_{d,\text{eff}}$ ) and the mid-plane temperature ( $T_d$ ) of the AGN disk evolve with  $R$ .  $\alpha = 0.01$ ,  $\epsilon_d = 0.1$ ,  $M_{\text{SMBH}} = 10^8 M_\odot$  and  $l_E = 0.5$  are adopted. The inner and outer boundaries of the disk are set to  $R_{\text{min}} = R_s/(4\epsilon_d)$  and  $R_{\text{max}} = 10^6 R_s$ , respectively.

between the two compact stars is taken as  $a_b = 10^{10}$  cm, below which the angular momentum loss in the binary is dominated by gravitational wave radiation (Tagawa et al. 2020).

The BCOs system can be regarded as a point source due to its comparably small size in the AGN disk. A circumbinary disk will form around the BCOs (Kimura et al. 2021). The viscosity parameter  $\alpha_b = 0.1$  and the height ratio  $h_b = H_b/r = 0.5$  are adopted to model the circumbinary disk.

Based on Bondi–Hölye–Lyttleton (BHL) model, Chen et al. (2023) discussed the formation and evolution of the circumbinary disk in the AGN disk. The outer boundary of the circumbinary disk is  $r_{\text{out}}$ , which can be estimated with the circularization radius  $r_{\text{cir}}$ . Applying the principle of conservation of angular momentum to the infalling gas, one has  $r_{\text{cir}} \times \sqrt{\frac{Gm_b}{r_{\text{cir}}}} = r_{\text{gra}} \times v_{\text{gra}}$ , where  $r_{\text{gra}} = \min\{r_{\text{BHL}}, r_{\text{Hill}}\}$  is the radius of the BCOs gravity sphere,  $v_{\text{gra}} \approx 1/2 r_{\text{gra}} \Omega_d$  is the velocity of the

gas at  $r_{\text{gra}}$ ,  $r_{\text{Hill}} = (m_b/3M_{\text{SMBH}})^{1/3} R_{\text{GRB}}$  is the Hill radius and  $r_{\text{BHL}} = Gm_b/c_s^2$  is the BHL radius (Edgar 2004). We find  $r_{\text{out}} \sim 4 \times 10^{12}$  cm.

The initial inflow mass rate at the outer boundary of the circumbinary disk  $\dot{m}_{\text{out}}$  is estimated with the BHL accretion rate and corrected for with the height of the AGN disk and the Hill radius,

$$\dot{m}_{\text{out}} = \dot{m}_{\text{BHL}} \times \min \left\{ 1, \frac{H}{r_{\text{BHL}}} \right\} \times \min \left\{ 1, \frac{r_{\text{Hill}}}{r_{\text{BHL}}} \right\}, \quad (7)$$

where  $\dot{m}_{\text{BHL}} = \frac{4\pi G^2 m_b^2 \rho_d}{c_s^3}$  is the BHL accretion rate.

We find  $\dot{m}_{\text{out}} \sim 10^7 \dot{m}_{\text{Edd}}$  with our parameter setup for the BCOs and AGN disk, and the Eddington accretion rate is  $\dot{m}_{\text{Edd}} = L_{\text{Edd,b}}/(\epsilon_b c^2)$ , where  $L_{\text{Edd,b}} = 4\pi Gm_b m_p c/\sigma_T$  is the Eddington luminosity. Photons will be trapped in such super-Eddington accretion flow in the inner region. The trapping radius is

$$r_{\text{tr}} = 3h_b \frac{\dot{m}_{\text{out}}}{\dot{m}_{\text{Edd}}} \frac{Gm_b}{c^2} = 3h_b \frac{\dot{m}_{\text{out}}}{\dot{m}_{\text{Edd}}} r_g \sim 2 \times 10^{13} \text{cm}, \quad (8)$$

where  $r_g = \frac{Gm_b}{c^2}$  is the gravitational radius of the BCOs.

The super-Eddington accretion disk will launch in a strong wind due to the influence of radiation pressure. The mass accretion rate onto BCOs will deviate from that at the outer boundary (Blandford & Begelman 1999),

$$\dot{m}_{\text{acc}} = \begin{cases} \dot{m}_{\text{out}}(r/r_{\text{tr}})^s, & r < r_{\text{tr}} \\ \dot{m}_{\text{out}}, & r > r_{\text{tr}} \end{cases}, \quad (9)$$

The parameter  $s$  describes the effects of wind, which varies from 0 to 1. The numerical simulations indicate that its value falls within the range 0.4 – 1.0. We therefore adopt  $s = 0.5$  in the calculations. The total luminosity of the wind is (Chen et al. 2023),

$$L_{\text{b,w}} = f_w \dot{m}_{\text{out,w}} c^2 \frac{r_g}{r_{\text{in,w}}} \left( \frac{r_{\text{in,w}}}{r_{\text{out,w}}} \right)^s \times \left[ \frac{1 - \left( \frac{r_{\text{in,w}}}{r_{\text{out,w}}} \right)^{1-s}}{1-s} - \frac{1 - \left( \frac{r_{\text{in,w}}}{r_{\text{out,w}}} \right)^{3/2}}{3/2} \right], \quad (10)$$

where  $f_w$  is the fraction of heat that is taken away by the disk wind,  $\dot{m}_{\text{out,w}}$  is the mass accretion rate at  $r_{\text{out,w}}$  of the circumbinary disk,  $r_{\text{in,w}}$  and  $r_{\text{out,w}}$  are the inner and outer boundaries of the wind launching region, respectively. We adopt  $r_{\text{in,w}} \sim 10r_g$  as the inner boundary. The outer boundary  $r_{\text{out,w}} = \min\{r_{\text{out}}, r_{\text{tr}}\} \sim r_{\text{out}}$ , then  $\dot{m}_{\text{out,w}} = \dot{m}_{\text{out}}(r_{\text{out,w}}/r_{\text{tr}})^s \approx 0.4\dot{m}_{\text{out}}$  and  $L_{\text{b,w}} \approx 5 \times 10^2 L_{\text{Edd,b}}$ .

The wind will expand consistently outwards in the accretion timescale  $t_{\text{acc}}$ , leading to a cavity in the AGN disk. As a result, the cavity will terminate the accretion, and the material from AGN disk will refill the cavity subsequently in a timescale  $t_{\text{ref}}$ . The accretion timescale  $t_{\text{acc}}$  can be estimated with the viscous timescale  $t_{\text{vis}}$  at  $r_{\text{out}}$ ,

$$t_{\text{acc}} \approx t_{\text{vis}}(r_{\text{out}}) = 1/(\alpha_b h_b^2 \Omega_{\text{K,b}}) \sim 8.7 \times 10^6 s, \quad (11)$$

where  $\Omega_{\text{K,b}} = \sqrt{Gm_b/r^3}$ .

The evolution of the wind's radius  $r_{\text{b,w}}$  and velocity  $v_{\text{b,w}}$  are (Weaver et al. 1977),

$$r_{\text{b,w}} = 0.88 \left( \frac{L_{\text{b,w}} t^3}{\rho_d} \right)^{1/5}, \quad (12)$$

$$v_{\text{b,w}} = 0.35 \left( \frac{L_{\text{b,w}}}{\rho_d t^2} \right)^{1/5}. \quad (13)$$

Now, we can investigate the possibility of SGRB progenitor wind penetrating from the AGN disk surface during the BCOs accretion timescale. By equating  $r_w = H$ , we can determine the penetrating timescale as  $\sim 0.2t_{\text{acc}}$ . The binary merger timescale due to gravitational wave radiation is denoted as (Shapiro & Teukolsky 1983),  $t_{\text{merge}} = \frac{5}{128} \frac{c^5 a_b^4}{G^3 m_b^3} \sim 3.9 \times 10^9 s \gg t_{\text{acc}}$ . Therefore, the wind can effectively penetrate the surface of the AGN disk prior to merger.

Wind velocity can be rewritten as  $v_{\text{b,w}} = 0.35(0.88/R_{\text{b,w}})^{2/3}(\rho_d/L_{\text{b,w}})^{-1/3}$ . The wind distribution is defined as

$$\rho_{\text{b,w}} \approx \frac{\dot{m}_w}{4\pi r_{\text{b,w}}^2 v_{\text{b,w}}} \approx \frac{\dot{m}_w (\rho_d/L_{\text{b,w}})^{1/3}}{4r_{\text{b,w}}^{4/3}}, \quad (14)$$

where  $\dot{m}_w = \dot{m}_{\text{out,w}} - \dot{m}_{\text{in,w}} \approx \dot{m}_{\text{out,w}}$  is the outflow rate of the disk wind and  $\dot{m}_{\text{in,w}}$  is the accretion rate at  $r_{\text{in,w}}$ .

The time scale for the cavity to be refilled by the dense gas in the AGN disk is approximately (Wang et al. 2021),

$$t_{\text{ref}} = H/c_s \sim 2 \times 10^7 s \approx 2t_{\text{acc}}. \quad (15)$$

The merger of BCOs can occur during either the accretion process or refill stage. The filled stage resembles the case discussed in Zhu et al. (2021), and is referred to as “no-cavity” in this work. In the subsequent calculations, we mainly focus on the penetrating case ( $r_{\text{b,cav}} = H$ ) for BCOs, and refer to it as “SGRB”.

### 2.2.2. Wind from LGRB progenitor

The progenitor of LGRBs is likely a Wolf-Rayet (WR) star (Woosley & Bloom 2006). The typical radius and effective temperature of WR stars are  $r_* = 5R_\odot$  and  $T_* = 10^5 K$ , respectively (Crowther 2007; Schaerer & Maeder 1992).

The wind luminosity can be written as,

$$L_{*,w} = \dot{m}_* v_\infty c, \quad (16)$$

where  $\dot{m}_*$  is the mass loss rate of the star and  $v_\infty$  is the terminal velocity of the wind. For WR stars,  $v_\infty \sim 1000 \text{ km/s}$  (Crowther 2007). The primary source of the stellar wind luminosity is the thermal radiation from the stellar surface. Therefore, we have

$$L_{*,w} \approx 4\pi r_*^2 \sigma_{\text{SB}} T_*^4. \quad (17)$$

According to Eqs. (16) and (17), one can derive that  $\dot{m}_* = \frac{4\pi r_*^2 \sigma_{\text{SB}} T_*^4}{v_\infty c}$ . The density distribution of the stellar wind  $\rho_{*,w}$  is

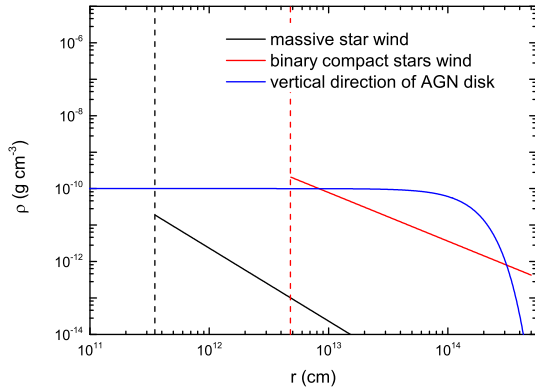


**Figure 2.** The density distribution of the LGRB progenitor (massive star) wind (black), the SGRB progenitor (BCOs) wind (red), and the AGN disk (blue) in vertical direction. The red and black dashed lines represent the inner boundaries of the BCOs wind and the massive star wind, respectively.

$$\rho_{*,w} \approx \frac{\dot{m}_*}{4\pi R^2 v_\infty}. \quad (18)$$

The wind will also develop a cavity in the AGN disk. The cavity size can be determined by considering the balance between the ram pressure of the stellar wind  $L_{*,w}/4\pi r^2 c$  and the thermal pressure of the AGN disk material  $P_d$ , i.e.,

$$r_{*,cav} = \sqrt{\frac{L_{*,w}}{4\pi c P_d}}, \quad (19)$$

which is  $\sim 0.05H$  for the parameters setting in this paper, and such case is referred to as ‘‘LGRB’’.

The reconstructed density profile surrounding the GRBs in AGN disk can be described with a piece-wise function,

$$\rho = \begin{cases} \rho_w, & r < r_{cav} \\ \rho_{AGN}, & r > r_{cav} \end{cases}, \quad (20)$$

where  $\rho_{AGN} = \rho_d \times \exp(-\frac{r^2}{2H^2})$  is the density distribution of the AGN disk in the vertical direction (Kathirgamaraju et al. 2023),  $\rho_w = \rho_{b,w}$  (or  $\rho_{*,w}$ ) for the case of SGRB (LGRB). The cavity size  $r_{cav} = 0$  for no-cavity case,  $H$  for SGRB case and  $0.05H$  for LGRB case.

Fig.2 presents the density profile for AGN disk (blue), BCO wind (red) and stellar wind (black). The vertical dashed lines represent the inner boundaries of progenitor wind ( $r_{0,w}$ ), i.e.,  $\sim 0.1r_{Hill} \approx 0.05H$  for SGRB case, and  $\sim r_*$  for LGRB case.

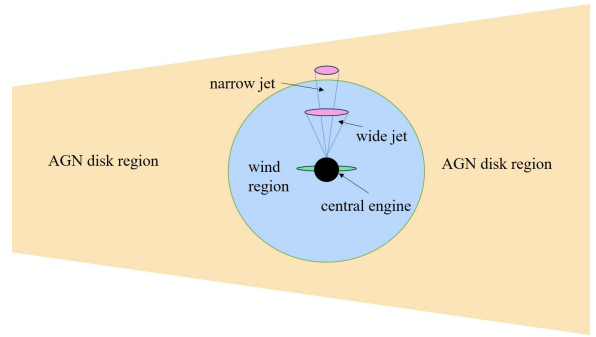


**Figure 3.** This schematic illustrates the structure of a jet and its surrounding environment within an AGN disk. The orange shaded region represents the AGN disk material, while the light blue region denotes the cavity developed by the GRB progenitor wind. We assume a GRB with a two components jet launched in mid-plane of the disk.

### 3. GRB WITH TWO-COMPONENT JET PROPAGATING IN THE AGN DISK

Now, we consider a GRB with a two-component jet that occurs in the accretion disk environment of an AGN with cavity, as shown in Fig. 3.

#### 3.1. Jet Dynamic in AGN Disk with Cavity

We consider a relativistic thin shell with isotropic energy  $E_{0,iso}$ , initial Lorentz factor  $\Gamma_0$ , and half-opening angle  $\theta_{j0}$  launched from the midplane of the AGN disk and directed perpendicularly to the disk plane, propagating into the ambient medium described in Section 2. The interaction between the shell and the medium is described by two shocks: a reverse shock (RS) propagating into the shell and a forward shock (FS) propagating into the ambient medium (Rees & Mészáros 2005; Piran 1999; Sari & Piran 1995). The two shocks divide the ambient medium and shell into four regions (Sari & Piran 1995): (1) the unshocked ambient medium region; (2) the shocked ambient medium region; (3) the shocked shell material region; (4) the unshocked shell material. First, the pair of shocks (FS and RS) propagate into the medium and the shell, respectively. After the RS crosses the shell, the blast wave enters the deceleration phase. After the blastwave has sufficiently decelerated, the shell enters the post-jet-break phase when the  $1/\Gamma$  cone exceeds  $\theta_j$ . The blastwave finally reaches the Newtonian phase the blast wave enters the Newtonian phase when it has swept up the ISM with the total rest mass energy comparable to the energy of the ejecta.

In the FS model, the dynamical evolution of the shell is calculated numerically using the equations (Huang et al. 2000; Pe'er 2012),

$$\frac{dr}{dt} = \beta c \Gamma \left( \Gamma + \sqrt{\Gamma^2 - 1} \right), \quad (21)$$

$$\frac{dm}{dr} = 2\pi r^2 (1 - \cos\theta_j) n_1 m_p, \quad (22)$$

$$\frac{d\theta_j}{dt} = \frac{c_{s,j} (\Gamma + \sqrt{\Gamma^2 - 1})}{R}, \quad (23)$$

$$\frac{d\Gamma}{dm} = - \frac{\hat{\gamma}(\Gamma^2 - 1) - (\hat{\gamma} - 1)\Gamma\beta^2}{m_{ej} + \epsilon m + (1 - \epsilon)m[2\hat{\gamma}\Gamma - (\hat{\gamma} - 1)(1 + \Gamma^{-2})]}, \quad (24)$$

where  $r$  and  $t$  are the radius and time of the jet in the source frame,  $\beta = \sqrt{\Gamma^2 - 1}/\Gamma$  is the dimensionless speed of the jet,  $m$  is the swept-up mass,  $n_1 = \rho/m_p$  is the medium density given by Eq. (20).  $m_{ej} = E_j/(\Gamma_0 c^2)$  is ejecta mass, and  $E_j = E_{0,iso}(1 - \cos\theta_{j0})$  is the kinetic energy of the ejecta.  $\epsilon$  is the radiative efficiency of the jet, and  $\epsilon = 0$  (adiabatic scenario) is adopted throughout this paper. Eq. (23) describes the side-way expanding of jet in the medium, where  $c_{s,j}$  is the sound speed of the shocked ambient medium which can be read as (Kirk & Duffy 1999),

$$c_{s,j}^2 = \frac{\hat{\gamma}(\hat{\gamma} - 1)(\Gamma - 1)}{1 + \hat{\gamma}(\Gamma - 1)} c^2, \quad (25)$$

where  $\hat{\gamma}$  is the adiabatic index. For simplicity, we adopt a polynomial fit formal to calculate the adiabatic index evolution the shocked ambient medium (Service 1986),  $\hat{\gamma} = (5 - 1.21937z + 0.18203z^2 - 0.96583z^3 + 2.32513z^4 - 2.39332z^5 + 1.07136z^6)/3$ , where  $z = \Theta/(0.24 + \Theta)$  and  $\Theta \simeq \frac{\Gamma\beta}{3} \frac{\Gamma\beta + 1.07(\Gamma\beta)^2}{1 + \Gamma\beta + 1.07(\Gamma\beta)^2}$ .

For the RS model, we adopted the theory developed by Kobayashi (2000). The RS is Newtonian in the thin shell scenario, namely  $\bar{\gamma}_{34} \sim 1$ , where  $\bar{\gamma}_{34}$  is the relative Lorentz factor between region (3) and region (4). The scalings before the time  $t_c$  of RS crossing the shell are,

$$\gamma_3 \simeq \Gamma_0, \quad n_3 \simeq 7n_1 \Gamma_0^2 \left( \frac{t}{t_c} \right)^{-3}, \quad (26)$$

$$e_3 \simeq \Gamma_0^2 n_1 m_p c^2, \quad N_{e,3} \simeq N_0 \left( \frac{t}{t_c} \right)^{3/2},$$

where  $\gamma_3$ ,  $n_3$ ,  $e_3$  and  $N_{e,3}$  are the Lorentz factor, comoving number density, energy density and the number of

electrons of Region 3.  $N_0 = M_{ej}/m_p$  is the total number of electrons in the shell. After the RS crossing, we have,

$$\begin{aligned} \gamma_3 &\propto t^{-g/(1+2g)}, \quad n_3 \propto t^{-6(3+g)/(7(1+2g))}, \\ e_3 &\propto t^{-8(3+g)/(7(1+2g))}, \quad N_{e,3} \simeq N_0. \end{aligned} \quad (27)$$

After  $t_c$ , the Lorentz factor of the shocked shell behaviors in a power-law decay  $\gamma_3 \propto r^{-g}$ , where the value of  $g$  depends on the density distribution of the external medium, e.g.,  $g \simeq 2$  for homogeneous medium and  $g \simeq 1$  for wind medium.

Zhu et al. (2021) pointed out that the GRB jet will be choked in the AGN disk. However, they did not consider the reconstruction of density profile due to the GRB progenitor wind. Therefore, we need to check whether the GRB jet can successfully break out from the AGN disk with cavity.

The jet could be choked if its tail catches up to the head. This occurs if  $(v_t - v_h)t_{j,bo} > z_j$ , or

$$t_{j,bo} > 2\Gamma^2 t_j, \quad (28)$$

where  $v_t$  and  $v_h$  are the tail and head velocity of the jet,  $t_{j,bo}$  is the timescale that the jet breakout from the AGN disk and  $z_j \approx ct_j$  is the length of the jet and  $t_j$  is the duration of the GRB.

The choked jet will then deposit its energy within the disk materials to form a hot cocoon with energy  $E_c \approx E_j$ . The cocoon undergoes expansion, leading to the formation of a radiation-mediated shock that sweeps through the AGN disk material until it ultimately breaks out.

### 3.2. Emission from Forward and Reverse Shocks

During the dynamical evolution of FS and RS, electrons are thought to be accelerated from the shock front by the first order Fermi acceleration mechanism to power-law distribution, i.e.,  $N(\gamma_e)d\gamma_e \propto \gamma_e^{-p}d\gamma_e$  ( $\gamma_m < \gamma_e < \gamma_M$ ), where  $\gamma_e$  is the Lorentz factor of the electrons and  $\gamma_m$  and  $\gamma_M$  are the minimum and maximum Lorentz factors of the injected electron (Sari 1998; Mészáros et al. 1998),

$$\gamma_m = \frac{g(p)\epsilon_e(\Gamma - 1)m_p}{m_e}, \quad (29)$$

where  $\epsilon_e$  is the fraction of the shock energy into electrons, and  $m_e$  is the mass of electron. The function  $g(p) = (p - 2)/(p - 1)$  for  $p > 2$ . The maximum electron

Lorentz factor  $\gamma_M$  can be calculated by balancing the acceleration and dynamical time scales,

$$\gamma_M \simeq \frac{\Gamma q_e B}{m_p c} t, \quad (30)$$

where  $q_e$  is the electron charge, and  $B$  is the comoving magnetic field strength,

$$B = \sqrt{8\pi e \epsilon_B}, \quad (31)$$

where  $e$  and  $\epsilon_B$  are the energy density in the shocked region and fraction of the shock energy in magnetic field. The observed radiation power for synchrotron radiation is (Rybicki & Lightman 1979),

$$P(\gamma_e) = \frac{4}{3} \sigma_T c \gamma_e^2 \frac{\Gamma^2 B^2}{8\pi}. \quad (32)$$

The characteristic frequency for an electron with Lorentz factor  $\gamma_e$  is,

$$\nu(\gamma_e) = \Gamma \gamma_e^2 \frac{q_e B}{2\pi m_e c}. \quad (33)$$

The peak power occurs at  $\nu(\gamma_e)$ ,

$$P_{\nu, \max} = \frac{P(\gamma_e)}{\nu(\gamma_e)} = \frac{m_e c^2 \sigma_T \Gamma B}{3q_e}. \quad (34)$$

The cooling Lorentz factor  $\gamma_c$  can be defined by equating the life time of a relativistic electron to the time  $t$ ,

$$\gamma_c = \frac{6\pi m_e c}{\Gamma \sigma_T B^2 t}, \quad (35)$$

While  $\gamma_e > \gamma_c$ , the cooling of the electrons would be significant, and further change the energy distribution of electrons. In synchrotron radiation, in addition to the characteristic frequencies  $\nu_m$  and  $\nu_c$ , there is an important characteristic frequency, self-absorption frequency  $\nu_a$ , which can be calculated by equating the synchrotron flux with the flux of a blackbody (Sari & Piran 1999; Kobayashi & Zhang 2003), or by the condition that the optical depth for self-absorption is unity (Rybicki & Lightman 1979).

The emissions from FS and RS are calculated by employing a modified version of the numerical code **PyFRS**<sup>2</sup> (Gao et al. 2013; Wang et al. 2014; Lei et al. 2016; Zhang 2018; Zhu et al. 2023; Zhou et al. 2024).

<sup>2</sup> <https://github.com/leiwH/PyFRS>

### 3.3. Diffused Emission

If the GRB jets are failed to penetrate the AGN disk surface, the FS and RS emission will be suppressed by radiation diffusion in the dense medium of AGN disk, which can significantly delay the emergence of the emission peak, turning the transient from FS and RS into a slow, isotropic, and dimmer one (Wang et al. 2022). In such case, the photosphere radius is  $r_{\text{ph}} \sim H$ .

The diffusion timescale is given by  $t_{\text{diff}} = r/c \int_{H-r}^H \kappa \rho dr$ .

The luminosity evolution of diffuse radiation can be represented by

$$L_{\text{diff}} = \frac{1}{t_{\text{diff}}} \exp\left(-\frac{t}{t_{\text{diff}}}\right) \int_0^t \exp\left(\frac{t'}{t_{\text{diff}}}\right) (L_{n,\text{in}} + L_{w,\text{in}}) dt' \quad (36)$$

The effective temperature can be expressed as,

$$T_{\text{eff}} = \left(\frac{L_{\text{diff}}}{4\pi r_{\text{ph}}^2 \sigma_{\text{SB}}}\right)^{1/4} \quad (37)$$

### 3.4. Cocoon shock breakout Emission

The cocoon shock breaks out when the dynamic timescale  $t_{\text{dyn},c} = d_c/v_c$  and diffusion timescale  $t_{\text{diff},c} = d_c/c \int_{H-d_c}^H \kappa_w \rho dR$  of the cocoon are equivalent. Therefore, the distance between the position of shock breakout and the AGN disk surface  $d_c$  can be obtained with  $t_{\text{diff},c} = t_{\text{dyn},c}$ . The mass of the breakout layer is  $m_c \approx \pi \rho \theta_c^2 H^2 d_c$ .

The total mass of the swept material by the cocoon when the shock breaks out is,

$$m_{\text{sw}} = \int_{r_{\text{ch}}}^H \pi \rho_w \theta_c^2 r^2 dr \quad (38)$$

where,  $r_{\text{ch}}$  is the position where the jet is choked. The velocity of the cocoon is  $v_c/c \approx \sqrt{1 - 1/\Gamma_c^2}$ , where  $\Gamma_c = E_c/m_{\text{sw}} c^2 + 1$ .

The energy released by the layer that the shock breaking out is  $E_{c,\text{bo}} = m_c c^2 (\Gamma_c - 1)$ , and the luminosity is,

$$L_{c,\text{bo}} = E_{c,\text{bo}}/t_{\text{diff},c}. \quad (39)$$

The duration of the shock breakout can be estimated as  $t_{\text{bo}} \approx (H - r_{\text{ch}})/v_c$ .

The radiation of the cocoon can be approximated as thermal radiation. If the velocity of the downstream of the cocoon shock  $v_c \gtrsim 0.1c$  the electrons and photons are in Compton (Katz et al. 2010). The cocoon temperature is  $T_c = (v_c/c)^{1/4} T_{\text{BB}} \eta^2 / \xi^2$ , where  $T_{\text{BB}} \approx \rho_c v_c^2 / a$

is the downstream temperature of the cocoon shock,  $\eta \approx 3 \times 10^{-36} \times \rho_c^{-1/8} v_c^{15/4}$  is the thermal coupling coefficient, and  $\xi = \max\{1, 0.5 \ln(y_{\max})(1.6 + \ln(y_{\max}))\}$  is the Comptonization correction factor.  $a$  is the radiation constant and  $y_{\max} \approx 2 \times 10^{-18} \times \rho_c^{-1/2} T_{\text{eff},c}^{9/4}$ . However, if  $v_c \sim c$ ,  $T_c \approx 4 \times 10^{13} E_a / (n_{\text{up}}^{1/2} \Gamma_c)$ , where  $n_{\text{up}} = \rho_{\text{up}} / m_p \text{ cm}^{-3}$  is the number density of the upstream of the cocoon shock,  $\Gamma_c = \sqrt{1/(1 - (v_c/c)^2)}$  is the Lorentz factor of the cocoon and  $E_a \approx 2 \times 10^{-34} \times (k_B T_c / (m_e c^2))^{-3/4} n_{\text{pair}}^{1/2} \text{ erg}$  is the absorption photon energy in the pair production equilibrium. The number density of pairs,  $n_{\text{pair}} \sim 1.7 \times 10^{-13} \times n_{\text{up}} \Gamma_c^2 (k_B T_c / (m_e c^2))^{-1} \beta_{\text{dn}}^{-2}$ , where  $\beta_{\text{dn}} \approx 0.3$  is the velocity of the downstream of the cocoon shock under the relativistic limit (Katz et al. 2010). Besides,  $\rho_{\text{up}} = \rho_{\text{dn}}$  for the jet choked in the AGN disk environment and  $\rho_{\text{up}} \sim \rho_{\text{b,w}}(r \sim H)$  for the jet choked in the wind from the disk of the binary compact stars.

#### 4. LIGHT CURVES, SPECTRA AND OBSERVABILITY

Now, we can calculate the emission from a GRB with two-component jet in AGN disk by considering the cavity produced by different progenitor wind model.

The parameters and values we adopted for the AGN disk and two-component jet are described in Table 1: the SMBH mass  $M_{\text{SMBH}}$ , the AGN disk height  $H$ , the mid-plane density of AGN disk  $\rho_d$ , the sound speed of disk  $c_s$ , the location of GRB in AGN disk  $R_{\text{GRB}}$ , the cavity size  $r_{\text{cav}}$ , the duration of GRB  $t_j$ , the initial Lorentz factor  $\Gamma_0$ , the initial half-opening angle  $\theta_{j0}$ , the isotropic kinetic energy  $E_{0,\text{iso}}$ , the fraction of the shock energy into electrons  $\epsilon_e$  and magnetic field  $\epsilon_B$ , and the electron energy distribution index  $p$ .

The dynamic evolution of the two-component jet (solid lines for narrow jet and dashed lines for wide one) are presented in Fig. 4 for SGRB and LGRB. The evolution of radius  $R$  and  $\Gamma\beta$  are plotted in the left and right panels, respectively. For comparison, we also show the results without cavity (black lines). We adopt  $t_j \sim 2s$  (30s) for SGRB (LGRB) case.

For the SGRB case, we consider cavity size  $r_{\text{cav}} \approx H$ . For the LGRB case,  $r_{\text{cav}} \approx 0.05H$  is adopted. We find that the results for the LGRB case roughly resemble the case without cavity, for which both the narrow and wide jets will be choked according to Eq. (28). For SGRB case, the narrow component would be choked,

**Table 1.** Parameters of AGN disk and GRB two-component jet

| AGN disk                       |                      |                      |
|--------------------------------|----------------------|----------------------|
| $M_{\text{SMBH}} (M_{\odot})$  | 10 <sup>8</sup>      |                      |
| $H$ (cm)                       | 10 <sup>14</sup>     |                      |
| $\rho_d$ (g cm <sup>-3</sup> ) | 10 <sup>-10</sup>    |                      |
| $c_s$ (cm s <sup>-1</sup> )    | 5 × 10 <sup>-6</sup> |                      |
| GRB and progenitor             |                      |                      |
|                                | SGRB                 | LGRB                 |
| $R_{\text{GRB}} (R_s)$         | 500                  | 1000                 |
| $r_{\text{cav}} (H)$           | 1                    | 0.05                 |
| $t_j$ (s)                      | 2                    | 30                   |
| Two-component jet              |                      |                      |
|                                | narrow               | wide                 |
| $\Gamma_0$                     | 300                  | 30                   |
| $\theta_{j0}$                  | 5°                   | 10°                  |
| $E_{0,\text{iso}}$ (erg)       | 2 × 10 <sup>52</sup> | 3 × 10 <sup>53</sup> |
| $\epsilon_e$                   | 0.3                  | 0.3                  |
| $\epsilon_B$                   | 0.01                 | 0.01                 |
| $p$                            | 2.3                  | 2.3                  |

but the wide component will successfully break out from the surface of the AGN disk due to  $t_{j,\text{bo}} < 2\Gamma_j^2 t_j \approx 60s$ . We would thus expect a non-thermal emission for such case.

##### 4.1. Light Curves

Based on the dynamics, we can calculate the emergent emission from the GRB in AGN disk.

In Fig.5, we present the emission of FS and RS (left panel) and the emergent emission (right panel) for no-cavity (top), SGRB (middle) and LGRB (bottom). For the emergent emission, we show the diffused emission, cocoon emission, and the emission from penetrated jet. For comparison, we also present the result for no-cavity and SGRB case in the result for LGRB case, see the bottom-right of Fig. 5.

It is found that, for both the FS/RS emission and their diffused emission, the early emission is dominated by the narrow component and the late emission by the wide component. The vertical magenta dotted line of represents the jet choked time. As discussed above, only the wide component in the SGRB case can successfully break out from the AGN disk surface. We therefore expect to observe a non-thermal FS emission peaking at  $5 \times 10^{45} \text{ erg s}^{-1}$  in this case, as shown with the green line

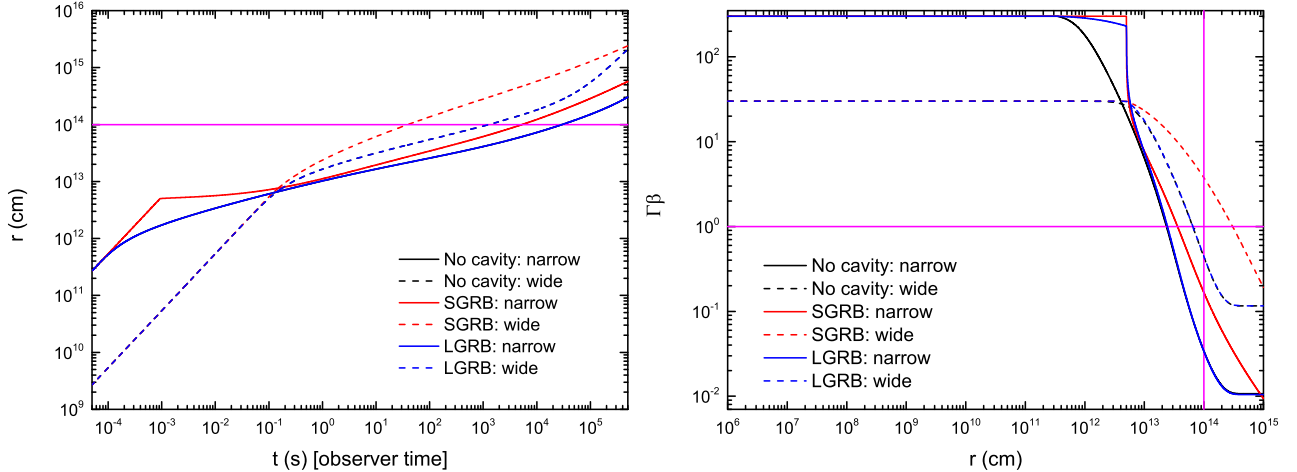


**Figure 4.** Dynamics of the narrow (solid lines) and wide (dashed lines) jets in the AGN disk for three cases, the no-cavity case (black), the SGRB case (red) and the LGRB case (blue). Left: the time evolution of the jet radius  $r$ . The horizontal magenta line represents the AGN disk surface; Right: the evolution of  $\Gamma\beta$  of the jet with  $r$ . The vertical and horizontal magenta lines represent the AGN disk surface and  $\Gamma\beta = 1$ , respectively.

in the middle-right panel. The diffused emission show a plateau with luminosity  $5 \times 10^{41} \text{ erg s}^{-1}$  and duration  $\sim 60$  days for LGRB and no-cavity cases, but with with luminosity  $\sim 5 \times 10^{43} \text{ erg s}^{-1}$  and duration  $\sim 0.7$  days for SGRB case.

The narrow (wide) cocoon emission for the cases of no-cavity and LGRB cases share similar breakout time  $\sim 12000 \text{ s}$  ( $\sim 2000 \text{ s}$ ), duration  $\sim 2800 \text{ s}$  ( $\sim 700 \text{ s}$ ) and luminosity  $\sim 1 \times 10^{46} \text{ erg s}^{-1}$  ( $\sim 5 \times 10^{48} \text{ erg s}^{-1}$ ). However, for the SGRB case, the narrow cocoon breaks out with breakout time  $\sim 900 \text{ s}$ , duration  $\sim 900 \text{ s}$  and luminosity  $\sim 5 \times 10^{46} \text{ erg s}^{-1}$ . One can find that the radiation of wide component cocoon are much brighter than the narrow component.

#### 4.2. Spectra and Observability

We further analyze the spectral characteristics and compare with that of the AGN disk. The results are shown in Fig. 6. We have computed the spectra of the AGN disk  $M_{\text{SMBH}} = 10^8 M_{\odot}$ .

We also calculate the possibility of detection in X-ray, soft gamma-ray, and optical bands by comparing with the thresholds of EP/WXT (Yuan 2017) EP/FXT (Yuan et al. 2015, 2022), g-band of WFST (Wang et al. 2023; Lei et al. 2023) and HXMT (Li 2007) in Fig. 6, respectively.

We found that, in all cases, the diffused emission is much dimmer than the AGN disk emission. The cocoon spectra for the LGRB is similar to those of the case without cavity. The temperatures of the diffused

and cocoon emission are labeled in the figures, i.e.,  $\sim 3 \times 10^7 \text{ K}$  for the diffused emission and  $\sim 3 \times 10^7 \text{ K}$  ( $\sim 3 \times 10^9 \text{ K}$ ) for the narrow (wide) cocoon. We also present the EP/WXT (red triangle), EP/FXT (green triangle), HXMT (blue triangle) and WFST (black triangle) sensitivity. The narrow and wide cocoons can be detected by EP and HXMT, respectively.

The radiation characteristics of SGRB are unique (see the lower left panel of Fig. 6). For comparison, we also show the narrow cocoon emission from the case without cavity, which is just the result of Zhu et al. (2021). The temperature for narrow cocoon in SGRB case is much higher than the no-cavity case, which can be monitored by HXMT. The wide jet can break out the AGN disk and contribute a non-thermal emission that can be detected by EP/FXT.

## 5. CONCLUSIONS AND DISCUSSIONS

In this work, we investigate the emission of a GRB with two-component jet in the AGN disk by considering the effects of progenitor wind on density distribution.

Our conclusions are summarized as follows:

1. Both progenitors (SGRBs and LGRBs) will develop a cavity in the AGN disk. The strong wind from the SGRB progenitors can penetrate the disk surface, while the LGRB progenitor can only produce a relatively small cavity.

2. Both the narrow and wide jets of the LGRBs will be choked in the disk, and the dynamical behaviors are similar to the case without cavity. However, for the

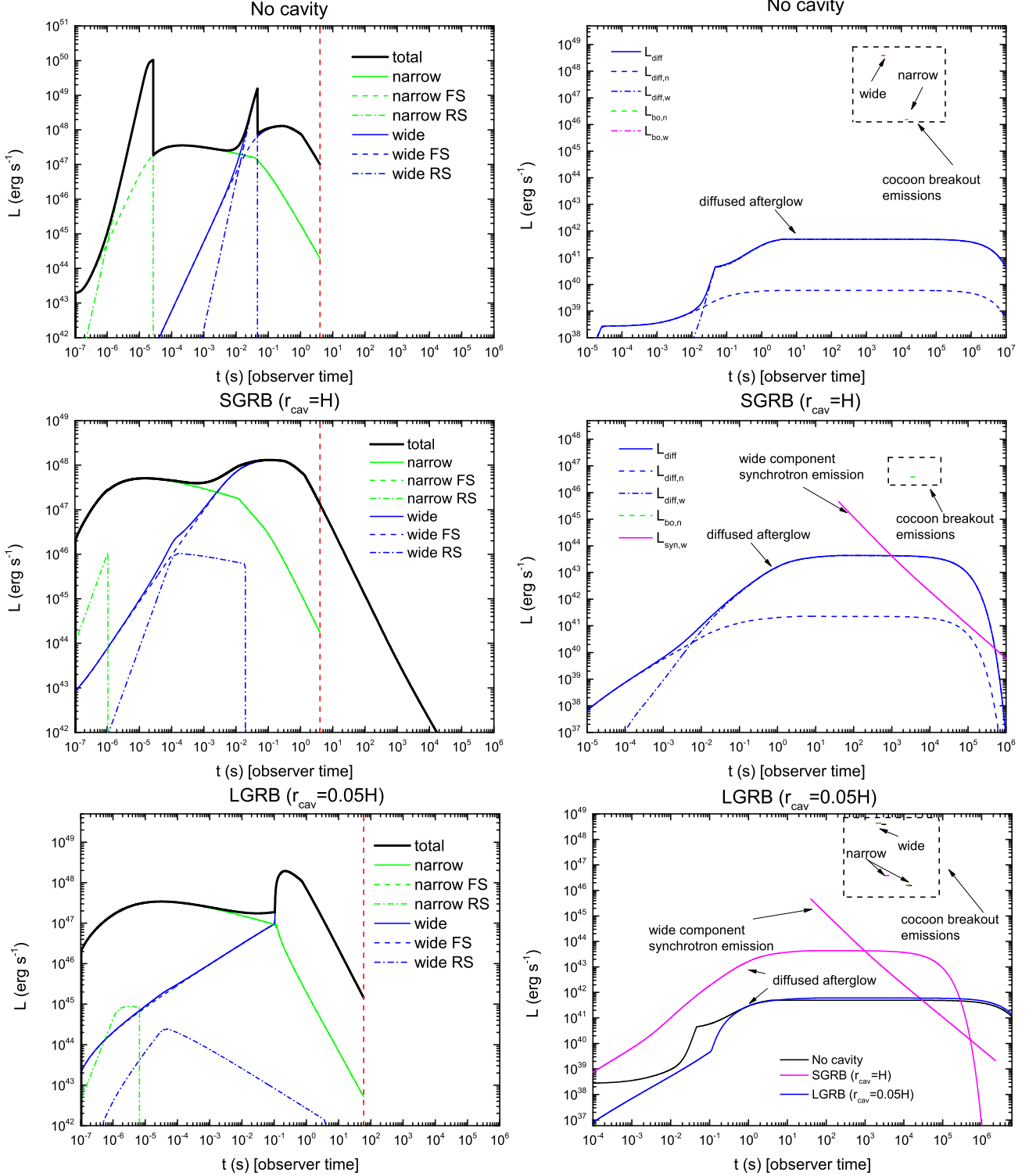


**Figure 5.** The left panel shows the FS luminosity (dashed lines), the RS luminosity (dotted-dashed lines) for the narrow (green) and the wide (blue) jets. The total jet-medium interaction luminosity is shown with black solid lines. The vertical dashed lines represent the jet choked time. The right panel shows the emergent emissions from a GRB in an AGN disk: the diffused luminosity, cocoon breakout luminosity and afterglow luminosity. Three cases, the no-cavity (top), SGRB ( $r_{\text{cav}}=H$ ) (middle) and LGRB ( $r_{\text{cav}}=0.05H$ ) (bottom) are considered. The comparison for these three cases is given in the bottom right panel.

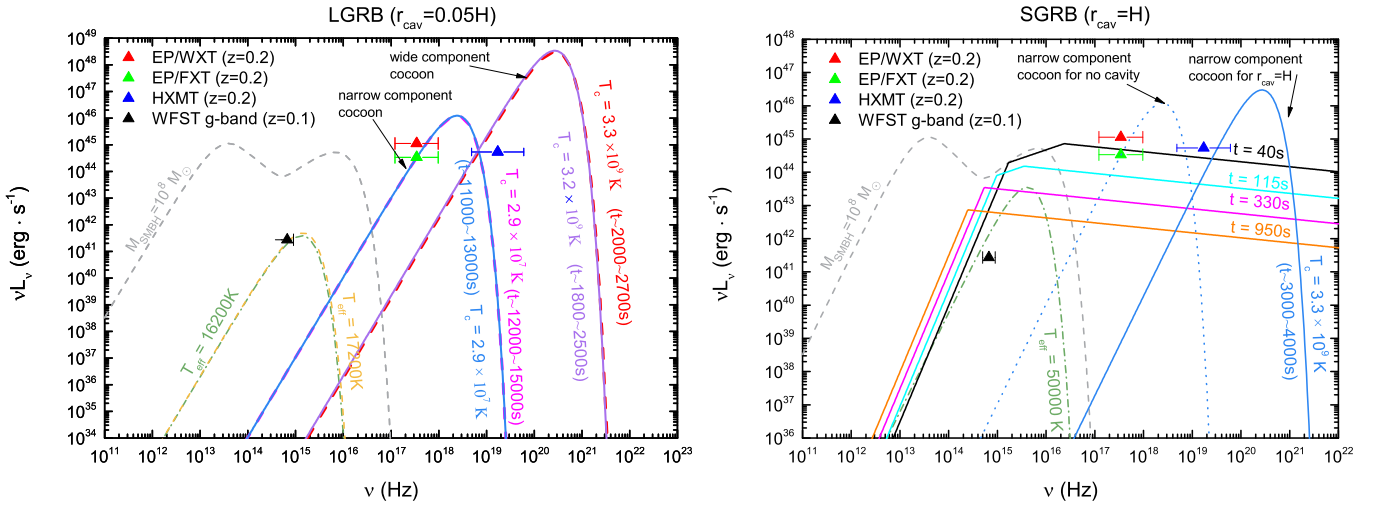


**Figure 6.** The spectra of the diffused (dotted-dashed lines), and the cocoon breakout (solid lines) for no-cavity (dashed lines) and LGRB (solid lines) cases in the left panel, and for the SGRB case in the right panel. For comparison, the AGN disk background are plotted with gray dashed lines. In the left panel, we compare the cocoon spectra of no-cavity (magenta dashed line for narrow component and red dashed line for wide component) and LGRB case (blue line for narrow component and purple line for wide component). In the right panel, we show the afterglow spectrum of the wide component jet. The time and the effective temperature of the spectra are also given. The different color triangles represent the sensitivity of EP/WXT, EP/FXT, WFST g-band and HXMT, respectively.

SGRBs, the wide jet can break out from the disk surface while the narrow jet will be choked in the cavity by the wind medium.

3. The emissions from the LGRBs and the no-cavity cases are similar. The SGRBs can produce brighter diffused emission, broad cocoon-breakout emission from narrow jet, and non-thermal emission from wide jet-breakout.

4. For all the cases, the diffused emission is much dimmer than the AGN disk background emission. However, the cocoon and non-thermal emission is much brighter. For the LGRBs and the case without cavity, the cocoon breakout emission from the narrow and wide jets can be detected by EP and HXMT, respectively. For the SGRBs in disk, the wide jet afterglow (non-thermal) emission and cocoon breakout emission from narrow jet can be monitored by EP and HXMT, respectively.

Therefore, the joint observations by EP and HXMT might be helpful to distinguish the type of GRBs in AGN disk and the jet components.

We have assumed that the progenitor winds are isotropic, and the jets are launched from the middle plane and perpendicular to the AGN disk. However, the wind could be angle dependent, which may be weak in polar direction for the SGRB case. The location of the jet launching and its orientation could be random in disk. The two-component jets launched near disk surface would produce a cocoon breakout emission and a non-thermal afterglow emission similar to the SGRB case discussed in this paper. The inclined jets or the precessing jet (Lei et al. 2007; Liu et al. 2010; Gao et al. 2023) would be difficult to break out of the disk surface, even in the SGRB case. The numerical simulations

would be helpful for detailed investigations (Kathiramaraju et al. 2023; Martin et al. 2024).

We adopted duration  $t_j = 2\text{s}$  for SGRBs. Traditionally,  $t_j \sim 2\text{s}$  is taken as the separation line for long and short GRBs. However, there are some merger-type GRBs with duration  $t_j > 2\text{s}$  (Gao et al. 2022). Therefore,  $t_j = 2$  could be a reasonable value for SGRBs. It should be noted that the GRBs may have late time central engine activities (Wu et al. 2013; Gao et al. 2016; Chen et al. 2017; Ma et al. 2018; Zhao et al. 2021; Huang et al. 2024), which would enhance the emissions (Huang et al. 2004).

Identification of GRBs in AGN disk is still challenging, especially considering other events with similar characteristics like tidal disruption events. However, strong gravitational wave signals are expected for these catastrophic events. In the future, we anticipate that ground and space gravitational wave detectors with higher sensitivity, such as the Einstein Telescope (Punturo et al. 2010a,b), Laser Interferometer Space Antenna (Amaro-Seoane et al. 2017), and TianQin (Amaro-Seoane et al. 2017), will detect more gravitational wave signals from AGN disks. Furthermore, neutrinos bursts could be detected by IceCube following the observation of gravitational wave (Zhu 2024). Therefore, multi-messenger follow-up observations are crucial for verifying the model proposed in this paper.

- 1 We are very grateful to Yaping Li, Hui Li, Fulin Li
- 2 and Bing Zhang for their helpful discussions. This
- 3 work is supported by the National Key R&D Program
- 4 of China (Nos. 2020YFC2201400, SQ2023YFC220007).
- 5 W.H.Lei. acknowledges support by the science research
- 6 grants from the China Manned Space Project with
- 7 NO.CMS-CSST-2021-B11.

## REFERENCES

- Abbott, R., Abbott, T. D., Abraham, S., et al. 2020, *PhRvL*, 125, 101102, doi: [10.1103/PhysRevLett.125.101102](https://doi.org/10.1103/PhysRevLett.125.101102)
- Abbott, R., Abbott, T. D., Acernese, F., et al. 2024, *PhRvD*, 109, 022001, doi: [10.1103/PhysRevD.109.022001](https://doi.org/10.1103/PhysRevD.109.022001)
- Amaro-Seoane, P., Audley, H., Babak, S., et al. 2017, arXiv e-prints, arXiv:1702.00786, doi: [10.48550/arXiv.1702.00786](https://doi.org/10.48550/arXiv.1702.00786)
- Artymowicz, P., Lin, D. N. C., & Wampler, E. J. 1993, *ApJ*, 409, 592, doi: [10.1086/172690](https://doi.org/10.1086/172690)
- Ashton, G., Ackley, K., Hernandez, I. M., & Piotrkowski, B. 2021, *Classical and Quantum Gravity*, 38, 235004, doi: [10.1088/1361-6382/ac33bb](https://doi.org/10.1088/1361-6382/ac33bb)
- Bellovary, J. M., Mac Low, M.-M., McKernan, B., & Ford, K. E. S. 2016, *ApJL*, 819, L17, doi: [10.3847/2041-8205/819/2/L17](https://doi.org/10.3847/2041-8205/819/2/L17)

- Berger, E., Kulkarni, S. R., Pooley, G., et al. 2003, *Nature*, 426, 154, doi: [10.1038/nature01998](https://doi.org/10.1038/nature01998)
- Blandford, R. D., & Begelman, M. C. 1999, *MNRAS*, 303, L1, doi: [10.1046/j.1365-8711.1999.02358.x](https://doi.org/10.1046/j.1365-8711.1999.02358.x)
- Branch, D., & Wheeler, J. C. 2017, *Supernova Explosions*, doi: [10.1007/978-3-662-55054-0](https://doi.org/10.1007/978-3-662-55054-0)
- Chatzopoulos, E., Wheeler, J. C., & Vinko, J. 2012, *ApJ*, 746, 121, doi: [10.1088/0004-637X/746/2/121](https://doi.org/10.1088/0004-637X/746/2/121)
- Chen, K., & Dai, Z.-G. 2024, *ApJ*, 961, 206, doi: [10.3847/1538-4357/ad0dfd](https://doi.org/10.3847/1538-4357/ad0dfd)
- Chen, K., Ren, J., & Dai, Z.-G. 2023, *ApJ*, 948, 136, doi: [10.3847/1538-4357/acc45f](https://doi.org/10.3847/1538-4357/acc45f)
- Chen, W., Xie, W., Lei, W.-H., et al. 2017, *ApJ*, 849, 119, doi: [10.3847/1538-4357/aa8f4a](https://doi.org/10.3847/1538-4357/aa8f4a)
- Crowther, P. A. 2007, *ARA&A*, 45, 177, doi: [10.1146/annurev.astro.45.051806.110615](https://doi.org/10.1146/annurev.astro.45.051806.110615)
- Dai, Z. G., & Gou, L. J. 2001, *ApJ*, 552, 72, doi: [10.1086/320463](https://doi.org/10.1086/320463)
- Dittmann, A. J., & Miller, M. C. 2020, *MNRAS*, 493, 3732, doi: [10.1093/mnras/staa463](https://doi.org/10.1093/mnras/staa463)
- Edgar, R. 2004, *NewAR*, 48, 843, doi: [10.1016/j.newar.2004.06.001](https://doi.org/10.1016/j.newar.2004.06.001)
- Fabj, G., Nasim, S. S., Caban, F., et al. 2020, *MNRAS*, 499, 2608, doi: [10.1093/mnras/staa3004](https://doi.org/10.1093/mnras/staa3004)
- Gao, H., Lei, W.-H., You, Z.-Q., & Xie, W. 2016, *ApJ*, 826, 141, doi: [10.3847/0004-637X/826/2/141](https://doi.org/10.3847/0004-637X/826/2/141)
- Gao, H., Lei, W.-H., & Zhu, Z.-P. 2022, *ApJL*, 934, L12, doi: [10.3847/2041-8213/ac80c7](https://doi.org/10.3847/2041-8213/ac80c7)
- Gao, H., Lei, W.-H., Zou, Y.-C., Wu, X.-F., & Zhang, B. 2013, *NewAR*, 57, 141, doi: [10.1016/j.newar.2013.10.001](https://doi.org/10.1016/j.newar.2013.10.001)
- Gao, H., Li, A., Lei, W.-H., & You, Z.-Q. 2023, *ApJ*, 945, 17, doi: [10.3847/1538-4357/acba0d](https://doi.org/10.3847/1538-4357/acba0d)
- Goodman, J. 2003, *MNRAS*, 339, 937, doi: [10.1046/j.1365-8711.2003.06241.x](https://doi.org/10.1046/j.1365-8711.2003.06241.x)
- Graham, M. J., Ford, K. E. S., McKernan, B., et al. 2020, *PhRvL*, 124, 251102, doi: [10.1103/PhysRevLett.124.251102](https://doi.org/10.1103/PhysRevLett.124.251102)
- Huang, B.-Q., Liu, T., Li, X.-Y., & Wei, Y.-F. 2024, *ApJ*, 967, 67, doi: [10.3847/1538-4357/ad3d54](https://doi.org/10.3847/1538-4357/ad3d54)
- Huang, Y. F., Gou, L. J., Dai, Z. G., & Lu, T. 2000, *ApJ*, 543, 90, doi: [10.1086/317076](https://doi.org/10.1086/317076)
- Huang, Y. F., Wu, X. F., Dai, Z. G., Ma, H. T., & Lu, T. 2004, *ApJ*, 605, 300, doi: [10.1086/382202](https://doi.org/10.1086/382202)
- Kathirgamaraju, A., Li, H., Ryan, B. R., & Tchekhovskoy, A. 2023, arXiv e-prints, arXiv:2311.03571, doi: [10.48550/arXiv.2311.03571](https://doi.org/10.48550/arXiv.2311.03571)
- Katz, B., Budnik, R., & Waxman, E. 2010, *ApJ*, 716, 781, doi: [10.1088/0004-637X/716/1/781](https://doi.org/10.1088/0004-637X/716/1/781)
- Kimura, S. S., Murase, K., & Bartos, I. 2021, *ApJ*, 916, 111, doi: [10.3847/1538-4357/ac0535](https://doi.org/10.3847/1538-4357/ac0535)
- Kirk, J. G., & Duffy, P. 1999, *Journal of Physics G Nuclear Physics*, 25, R163, doi: [10.1088/0954-3899/25/8/201](https://doi.org/10.1088/0954-3899/25/8/201)
- Kobayashi, S. 2000, *ApJ*, 545, 807, doi: [10.1086/317869](https://doi.org/10.1086/317869)
- Kobayashi, S., & Zhang, B. 2003, *ApJL*, 582, L75, doi: [10.1086/367691](https://doi.org/10.1086/367691)
- Lei, L., Zhu, Q.-F., Kong, X., et al. 2023, *Research in Astronomy and Astrophysics*, 23, 035013, doi: [10.1088/1674-4527/acb877](https://doi.org/10.1088/1674-4527/acb877)
- Lei, W. H., Wang, D. X., Gong, B. P., & Huang, C. Y. 2007, *A&A*, 468, 563, doi: [10.1051/0004-6361:20066219](https://doi.org/10.1051/0004-6361:20066219)
- Lei, W.-H., Yuan, Q., Zhang, B., & Wang, D. 2016, *ApJ*, 816, 20, doi: [10.3847/0004-637X/816/1/20](https://doi.org/10.3847/0004-637X/816/1/20)
- Li, F.-L., Liu, Y., Fan, X., et al. 2023, *ApJ*, 950, 161, doi: [10.3847/1538-4357/acd2d1](https://doi.org/10.3847/1538-4357/acd2d1)
- Li, T.-P. 2007, *Nuclear Physics B Proceedings Supplements*, 166, 131, doi: [10.1016/j.nuclphysbps.2006.12.070](https://doi.org/10.1016/j.nuclphysbps.2006.12.070)
- Lin, D. N. C., & Papaloizou, J. C. B. 1993, in *Protostars and Planets III*, ed. E. H. Levy & J. I. Lunine, 749
- Liu, T., Liang, E. W., Gu, W. M., et al. 2010, *A&A*, 516, A16, doi: [10.1051/0004-6361/200913447](https://doi.org/10.1051/0004-6361/200913447)
- Lynden-Bell, D. 1969, *Nature*, 223, 690, doi: [10.1038/223690a0](https://doi.org/10.1038/223690a0)
- Ma, S.-B., Lei, W.-H., Gao, H., et al. 2018, *ApJL*, 852, L5, doi: [10.3847/2041-8213/aaa0cd](https://doi.org/10.3847/2041-8213/aaa0cd)
- Maeder, A. 1983, *A&A*, 120, 113
- Martin, R. G., Lepp, S., Zhang, B., Nixon, C. J., & Childs, A. C. 2024, *MNRAS*, 528, L161, doi: [10.1093/mnras/sl4174](https://doi.org/10.1093/mnras/sl4174)
- McKernan, B., Ford, K. E. S., Bartos, I., et al. 2019, *ApJL*, 884, L50, doi: [10.3847/2041-8213/ab4886](https://doi.org/10.3847/2041-8213/ab4886)
- Mészáros, P., Rees, M. J., & Wijers, R. A. M. J. 1998, *ApJ*, 499, 301, doi: [10.1086/305635](https://doi.org/10.1086/305635)
- Morton, S. L., Rinaldi, S., Torres-Orjuela, A., et al. 2023, *PhRvD*, 108, 123039, doi: [10.1103/PhysRevD.108.123039](https://doi.org/10.1103/PhysRevD.108.123039)
- Nitz, A., & Capano, C. 2020, *gwastro/2-ogc: V1.0 of 2-OGC data release, v1.0*, Zenodo, doi: [10.5281/zenodo.3630644](https://doi.org/10.5281/zenodo.3630644)
- Paczynski, B. 1978, *AcA*, 28, 91
- Pe'er, A. 2012, *ApJL*, 752, L8, doi: [10.1088/2041-8205/752/1/L8](https://doi.org/10.1088/2041-8205/752/1/L8)
- Perna, R., Lazzati, D., & Cantiello, M. 2021, *ApJL*, 906, L7, doi: [10.3847/2041-8213/abd319](https://doi.org/10.3847/2041-8213/abd319)
- Piran, T. 1999, *PhR*, 314, 575, doi: [10.1016/S0370-1573\(98\)00127-6](https://doi.org/10.1016/S0370-1573(98)00127-6)
- Punturo, M., Abernathy, M., Acernese, F., et al. 2010a, *Classical and Quantum Gravity*, 27, 084007, doi: [10.1088/0264-9381/27/8/084007](https://doi.org/10.1088/0264-9381/27/8/084007)
- . 2010b, *Classical and Quantum Gravity*, 27, 194002, doi: [10.1088/0264-9381/27/19/194002](https://doi.org/10.1088/0264-9381/27/19/194002)
- Rees, M. J., & Mészáros, P. 2005, *ApJ*, 628, 847, doi: [10.1086/430818](https://doi.org/10.1086/430818)

- Rybicki, G. B., & Lightman, A. P. 1979, Radiative processes in astrophysics
- Sari, R. 1998, ApJL, 494, L49, doi: [10.1086/311160](https://doi.org/10.1086/311160)
- Sari, R., & Piran, T. 1995, ApJL, 455, L143, doi: [10.1086/309835](https://doi.org/10.1086/309835)
- . 1999, ApJ, 520, 641, doi: [10.1086/307508](https://doi.org/10.1086/307508)
- Schaerer, D., & Maeder, A. 1992, A&A, 263, 129
- Service, A. T. 1986, ApJ, 307, 60, doi: [10.1086/164392](https://doi.org/10.1086/164392)
- Shakura, N. I., & Sunyaev, R. A. 1973, A&A, 24, 337
- Shapiro, S. L., & Teukolsky, S. A. 1983, Black holes, white dwarfs and neutron stars. The physics of compact objects, doi: [10.1002/9783527617661](https://doi.org/10.1002/9783527617661)
- Sheth, K., Frail, D. A., White, S., et al. 2003, ApJL, 595, L33, doi: [10.1086/378933](https://doi.org/10.1086/378933)
- Sirko, E., & Goodman, J. 2003, MNRAS, 341, 501, doi: [10.1046/j.1365-8711.2003.06431.x](https://doi.org/10.1046/j.1365-8711.2003.06431.x)
- Tagawa, H., Haiman, Z., & Kocsis, B. 2020, ApJ, 898, 25, doi: [10.3847/1538-4357/ab9b8c](https://doi.org/10.3847/1538-4357/ab9b8c)
- Tagawa, H., Kimura, S. S., Haiman, Z., Perna, R., & Bartos, I. 2024, ApJ, 966, 21, doi: [10.3847/1538-4357/ad2e0b](https://doi.org/10.3847/1538-4357/ad2e0b)
- Tetarenko, B. E., Lasota, J. P., Heinke, C. O., Dubus, G., & Sivakoff, G. R. 2018, Nature, 554, 69, doi: [10.1038/nature25159](https://doi.org/10.1038/nature25159)
- Wang, J.-M., Liu, J.-R., Ho, L. C., & Du, P. 2021, ApJL, 911, L14, doi: [10.3847/2041-8213/abee81](https://doi.org/10.3847/2041-8213/abee81)
- Wang, J.-Z., Lei, W.-H., Wang, D.-X., et al. 2014, ApJ, 788, 32, doi: [10.1088/0004-637X/788/1/32](https://doi.org/10.1088/0004-637X/788/1/32)
- Wang, T., Liu, G., Cai, Z., et al. 2023, Science China Physics, Mechanics, and Astronomy, 66, 109512, doi: [10.1007/s11433-023-2197-5](https://doi.org/10.1007/s11433-023-2197-5)
- Wang, Y.-H., Lazzati, D., & Perna, R. 2022, MNRAS, 516, 5935, doi: [10.1093/mnras/stac1968](https://doi.org/10.1093/mnras/stac1968)
- Weaver, R., McCray, R., Castor, J., Shapiro, P., & Moore, R. 1977, ApJ, 218, 377, doi: [10.1086/155692](https://doi.org/10.1086/155692)
- Woosley, S. E. 1993, in American Astronomical Society Meeting Abstracts, Vol. 182, American Astronomical Society Meeting Abstracts #182, 55.05
- Woosley, S. E., & Bloom, J. S. 2006, ARA&A, 44, 507, doi: [10.1146/annurev.astro.43.072103.150558](https://doi.org/10.1146/annurev.astro.43.072103.150558)
- Wu, X. F., Dai, Z. G., Huang, Y. F., & Lu, T. 2005, MNRAS, 357, 1197, doi: [10.1111/j.1365-2966.2005.08685.x](https://doi.org/10.1111/j.1365-2966.2005.08685.x)
- Wu, X.-F., Hou, S.-J., & Lei, W.-H. 2013, ApJL, 767, L36, doi: [10.1088/2041-8205/767/2/L36](https://doi.org/10.1088/2041-8205/767/2/L36)
- Xie, W., Lei, W.-H., Zou, Y.-C., et al. 2012, Research in Astronomy and Astrophysics, 12, 817, doi: [10.1088/1674-4527/12/7/010](https://doi.org/10.1088/1674-4527/12/7/010)
- Xu, C., Baum, S. A., O'Dea, C. P., Wrobel, J. M., & Condon, J. J. 2000, AJ, 120, 2950, doi: [10.1086/316842](https://doi.org/10.1086/316842)
- Yuan, W. 2017, in 7 years of MAXI: monitoring X-ray Transients, ed. M. Serino, M. Shidatsu, W. Iwakiri, & T. Mihara, 247
- Yuan, W., Zhang, C., Chen, Y., & Ling, Z. 2022, in Handbook of X-ray and Gamma-ray Astrophysics, 86, doi: [10.1007/978-981-16-4544-0\\_151-1](https://doi.org/10.1007/978-981-16-4544-0_151-1)
- Yuan, W., Zhang, C., Feng, H., et al. 2015, arXiv e-prints, arXiv:1506.07735, doi: [10.48550/arXiv.1506.07735](https://doi.org/10.48550/arXiv.1506.07735)
- Zhang, B. 2018, The Physics of Gamma-Ray Bursts, doi: [10.1017/9781139226530](https://doi.org/10.1017/9781139226530)
- Zhang, W., Woosley, S. E., & Heger, A. 2004, ApJ, 608, 365, doi: [10.1086/386300](https://doi.org/10.1086/386300)
- Zhao, L., Gao, H., Lei, W., Lan, L., & Liu, L. 2021, ApJ, 906, 60, doi: [10.3847/1538-4357/abc8ec](https://doi.org/10.3847/1538-4357/abc8ec)
- Zheng, J.-H., Wang, X.-Y., Liu, R.-Y., & Zhang, B. 2024, ApJ, 966, 141, doi: [10.3847/1538-4357/ad3949](https://doi.org/10.3847/1538-4357/ad3949)
- Zhou, C., Zhu, Z.-P., Lei, W.-H., et al. 2024, ApJ, 963, 66, doi: [10.3847/1538-4357/ad20f3](https://doi.org/10.3847/1538-4357/ad20f3)
- Zhu, J.-P. 2024, MNRAS, 528, L88, doi: [10.1093/mnras/sl4d176](https://doi.org/10.1093/mnras/sl4d176)
- Zhu, J.-P., Zhang, B., Yu, Y.-W., & Gao, H. 2021, ApJL, 906, L11, doi: [10.3847/2041-8213/abd412](https://doi.org/10.3847/2041-8213/abd412)
- Zhu, Z.-P., Xu, D., Fynbo, J. P. U., et al. 2023, ApJ, 948, 30, doi: [10.3847/1538-4357/acbd96](https://doi.org/10.3847/1538-4357/acbd96)